



Synthesis and characterization of highly conductive plasticized double core organic–inorganic hybrid electrolytes for lithium polymer batteries



Hao-Yiang Wu^a, Diganta Saikia^b, Hung-Yu Chao^b, Yu-Chi Pan^b, Jason Fang^c,
Li-Duan Tsai^c, George T.K. Fey^d, Hsien-Ming Kao^{b,*}

^a Department of Neurological Surgery, Tri-Service General Hospital, National Defense Medical Center, 325, Sec. 2, Cheng-Kung Rd, Nei-Hu Dist, Taipei 11490, Taiwan, ROC

^b Department of Chemistry, National Central University, Jhongli, Taiwan 32054, ROC

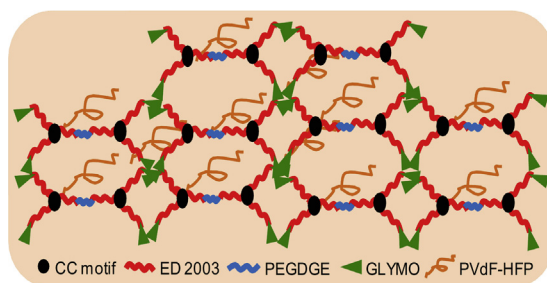
^c Department of Fuel Cell Materials and Advanced Capacitors, Division of Energy Storage Materials and Technology, Material and Chemical Laboratories, Industrial Technology Research Institute, Hsin-Chu 300, ROC

^d Department of Chemical and Materials Engineering, National Central University, Jhongli, Taiwan 32054, ROC

HIGHLIGHTS

- Organic–inorganic hybrid membrane has been synthesized by sol–gel process.
- Hybrid membrane was evaluated with different electrolyte solvents.
- Plasticized hybrid electrolyte membrane possessed maximum swelling ratio of 794%.
- Maximum ionic conductivity of 6.9 mS cm^{-1} was achieved with the electrolyte membrane.
- Test cell shows initial discharge capacity of 115 mAh g^{-1} .

GRAPHICAL ABSTRACT



ARTICLE INFO

Article history:

Received 8 November 2012

Received in revised form

25 February 2013

Accepted 7 March 2013

Available online 26 March 2013

Keywords:

Organic–inorganic hybrid electrolyte

Ionic conductivity

Swelling ratio

Discharge capacity

Lithium polymer battery

ABSTRACT

A new highly ion conductive plasticized organic–inorganic hybrid electrolyte membrane based on tri-block co-polymer poly(propylene glycol)-*block*-poly(ethylene glycol)-*block*-poly(propylene glycol) bis(2-aminopropyl ether) (ED2003), poly(ethylene glycol) diglycidyl ether (PEGDGE), poly(vinylidene fluoride-co-hexafluoropropylene) (PVdF–HFP), 2,4,6-trichloro-1,3,5-triazine (cyanuric chloride, CC) and 3-(glycidyloxypropyl)trimethoxysilane (GLYMO) has been synthesized by a sol–gel process and characterized by a variety of experimental techniques. FTIR and ^{13}C NMR measurements have been performed to study the molecular structure of the hybrid as well as the interactions among the constituents of the membrane. The hybrid membrane is plasticized with different electrolyte solvents and exhibits remarkable swelling ratios in the range of 670–800%. The ionic conductivity of the hybrid electrolyte membranes is varied with different electrolyte solvents and shows a maximum value of $6.9 \times 10^{-3} \text{ S cm}^{-1}$ for 1 M LiClO_4 in EC/PC at 30°C . The test cell carries initial discharge capacity of 115 mAh g^{-1} at a current rate of 0.2 C and shows good cycling performance up to 100 cycles and coulombic efficiency of 98–99% for the entire cycles. The plasticized organic–inorganic hybrid electrolyte membrane holds promise for applications in lithium polymer batteries.

© 2013 Elsevier B.V. All rights reserved.

* Corresponding author. Tel.: +886 3 4275054; fax: +886 3 4227664.

E-mail address: hmkao@cc.ncu.edu.tw (H.-M. Kao).

1. Introduction

The urgent need for batteries with high power and energy densities increases the demand for advanced lithium-ion battery technology due to its numerous applications in electronic gadgets to hybrid electric vehicles [1–4]. Electrolytes play a pivotal role in the fabrication of high power batteries. Particularly, ion-conducting polymer electrolyte membranes are very promising for lithium polymer batteries [5–8]. To be an ideal electrolyte, it should possess high ionic conductivity (10^{-3} – 10^{-2} S cm $^{-1}$), mechanically, electrochemically and thermally stable, and should be processed as an ultrathin film. Liquid electrolytes that are used in the fabrication of conventional batteries have problems of internal shorting, leakage, highly reactive nature toward electrodes, and bigger size container to store the electrolyte, leading to the increase in the size of the battery. In contrast, the lithium-ion batteries currently use thin (e.g., 25 μ m) microporous polyolefin separators, but the cost of these separators is significantly higher which increases the overall manufacturing cost of the Li-ion batteries. Moreover, polyolefin separators show poor wetting capability because of their small pore size and porosity, which hinder the absorption of electrolyte solutions into the microporous membrane [9]. The use of polymer electrolyte can give a porous separator with controllable pore size and a cost effective, light weight, leak proof and flexible battery. Recently, many works are going on to improve the properties of polymer electrolytes [9–12]. Solid polymer electrolytes (SPEs) promise the potential to replace organic liquid electrolytes and thereby improve the safety of next-generation high-energy batteries [13–15]. However, their low ionic conductivities have restricted the mass use of this type of electrolytes in batteries [16–18]. Some approaches such as addition of micron/nano-sized filler particles, use of co-polymers and blends, synthesis of crosslinked and branched structure, use of organic solvents in polymer matrices (gel or plasticized electrolytes), etc. have been tested and succeeded to enhance the ionic conductivity [19–23]. Among these approaches, gel or plasticized polymer electrolytes (GPEs/PPEs) are regarded as prospective alternative for traditional liquid electrolytes used in batteries, since PPEs are considered to be an intermediate state between liquid electrolytes and solid polymer electrolytes. The electrolyte leakage from a battery can be to a large extent prevented with this gel or plasticized electrolytes as the liquid component is trapped in the polymer matrix and therefore the membrane virtually looks like a solid in character. Moreover, ionic conductivities of the GPEs or PPEs are comparable to the liquid electrolytes used in the lithium ion batteries [10,24–26].

Many different polymers are investigated as possible gel matrices [22–28]. Among them, organic–inorganic hybrid materials are advantageous as matrices due to the easy control of the properties of the final material by controlling the chemical nature of the organic and inorganic phases, the size and morphology of these domains (nm to sub- μ m scale) and the nature of the interphase interactions. The sol–gel process is a useful method to synthesize these materials because it allows a wide variation in compositions and inorganic/organic ratios, together with an excellent control of porosity (volume, size and connectivity) and functional groups. These features enable the design of hybrid materials to serve as electrolytes for lithium ion batteries. Although many researchers have been working on this type of hybrid electrolytes for possible applications, most of them have attempted with solvent free hybrid electrolytes, which generally have conductivities in the range of 10^{-5} to 10^{-4} S cm $^{-1}$ [29–33]. Relatively few papers have reported the use of plasticized organic–inorganic hybrid electrolytes for possible applications in lithium ion batteries [27,34].

With the above objectives, here we report a new type of plasticized organic–inorganic hybrid electrolyte for possible applications

in lithium polymer batteries. The hybrid electrolyte was synthesized by the reaction of 2,4,6-trichloro-1,3,5-triazine (cyanuric chloride, CC) with poly(propylene glycol)-*block*-poly(ethylene glycol)-*block*-poly(propylene glycol) bis(2-aminopropyl ether) (ED2003), followed by the reaction with poly(ethylene glycol) diglycidyl ether (PEGDGE). Cyanuric chloride was chosen because of its ability to form star-branched structure. 3-(Glycidyloxypropyl)trimethoxysilane (GLYMO) was further added to react with the amine end groups of ED2003 to form the silicate network in the hybrid structure. Silicate network makes the membrane mechanically stable and gives a composite nature to the membrane by forming *in-situ* sub-micron sized particles. To further enhance the mechanical properties, a small amount of poly(vinylidene fluoride-co-hexafluoropropylene) (PVdF–HFP) was added in the synthesis process of the membrane. PVdF–HFP is also advantageous because of its good electrochemical stability with respect to nonaqueous electrolytes and electrode materials [35–37]. The synthesized organic–inorganic hybrid membrane was evaluated with different electrolyte solvents. The structural and electrochemical properties of the hybrid electrolyte membrane thus obtained were systematically investigated by a variety of techniques including Fourier transform infrared spectroscopy (FTIR), thermogravimetric analysis (TGA), 13 C solid-state NMR, AC impedance, linear sweep voltammetry (LSV) and charge–discharge measurements.

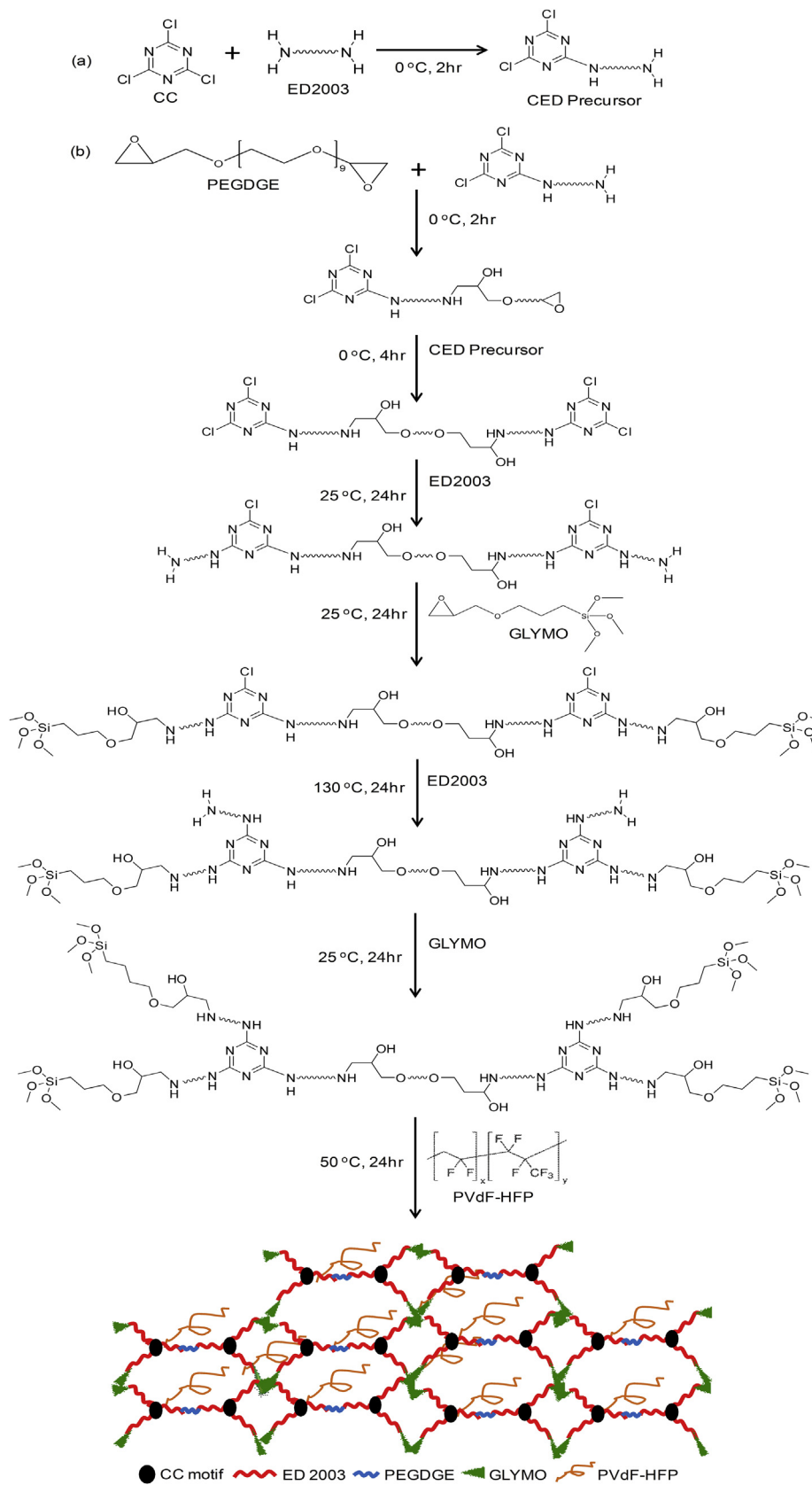
2. Experimental

2.1. Materials

Triblock copolymer H $_2$ N–(PPG) $_x$ (PEG) $_y$ (PPG) $_z$ NH $_2$ (commercially designated by Jeffamine ED2003 with $M_w = 2000$ g mol $^{-1}$ containing $x + z = 6$; $y = 39$), PVdF–HFP ($M_w = 400,000$ g mol $^{-1}$), PEGDGE, lithium perchlorate (LiClO $_4$), lithium bis(trifluoromethylsulfonyl) imide (LiTFSI) and lithium trifluoromethanesulfonate (LiOTf) were purchased from Aldrich company. Ethylene carbonate (EC) and propylene carbonate (PC) were obtained from Alfa Aesar. Electrolyte 1 M LiPF $_6$ in EC/diethyl carbonate (DEC) was acquired from Tomiyama Chemicals, Japan. Cyanuric chloride (denoted as CC, obtained from Aldrich), and GLYMO (Aldrich) were used as received. Tetrahydrofuran (THF) was distilled from sodium/benzophenone prior to use. The cathode materials nickel manganese cobalt oxide (NMC442) and LiMn $_2$ O $_4$ (LMO) were provided by Industrial Technology Research Institute (ITRI), Taiwan.

2.2. Preparation of double core organic–inorganic hybrid electrolyte membranes

To prepare the hybrid membrane, ED2003 was dried under vacuum for 2 days prior to use. Scheme 1 illustrates the synthesis procedures of the double core organic–inorganic hybrid membrane. Based on the temperature dependence of the reaction selectivity of the three chlorine atoms in CC, the reactions were performed at three different temperatures, namely at 0, 25 (room temperature), and 130 °C. In the first step, 0.75 mmol of ED2003 and CC were dissolved in a small amount of THF separately and then mixed together and stirred at 0 °C for 2 h to form the CED precursor. 0.75 mmol of PEGDGE was added to the solution and continuously stirred at 0 °C for another 2 h. Again, 0.75 mmol of the CED precursor was added to the above solution at 0 °C and stirred for another 4 h to form the linear structure, as shown in Scheme 1. In the second step, the temperature of the solution was raised to room temperature and 1.5 mmol (two times of 0.75 mmol) of ED2003 was added and stirred for 24 h to replace the second Cl atom from both CC core and react with one end of amine group.



Scheme 1. Synthesis and structure of organic–inorganic hybrid membranes.

After that, 1.5 mmol of GLYMO was added and stirred for another 24 h at room temperature to react with another amine end group of the ED2003. In the third step, the temperature of the mixed solution was raised to 130 °C and 1.5 mmol of ED2003 was added and stirred for 24 h to replace the third Cl atom from both CC core. Afterward, temperature was brought down to room temperature and 1.5 mmol of GLYMO was added to the mixture and stirred for 24 h to react with the amine end group of ED2003 and form the double core branched structure. Finally, 5–10 wt.% of PVdF–HFP (dissolved in THF at 50 °C) was added into the mixed solution and stirred continuously at same temperature for 24 h. Reaction temperature of 50 °C was chosen for thorough mixing of both solutions. The resulting viscous solution was casted onto Teflon dishes and dried in a vacuum oven to get mechanically stable and flexible membrane. Membranes were stored in argon atmosphere inside a glove box (Innovative technology, PL-HE-2GB with PL-HE-GP1 inert gas purifier) for further characterization. The synthesized hybrid membranes were plasticized with various electrolyte solvents, such as 1 M LiClO₄ in EC/PC (1:1, v/v), 1 M LiOTf in EC/PC (1:1, v/v), 1 M LiTFSI in EC/PC (1:1, v/v) and 1 M LiPF₆ in EC/DEC (1:1, v/v). The membranes thus obtained were denoted as PCEG-Y, where P represents the PEGDGE, C stands for cyanuric chloride, E corresponds to ED2003, G for GLYMO and Y indicates the percentage weight ratio of PVdF–HFP/total amount of ED2003 added per CC. The membrane thickness was controlled in the range of 50–80 μm.

2.3. Characterization methods

The FTIR spectra were obtained from a Bio-Rad FTS155 spectrometer over the range of 4000–400 cm⁻¹ at a resolution of 4 cm⁻¹ using the KBr wafer technique. Solid-state NMR experiments were performed on a Varian Infinityplus-500 NMR spectrometer equipped with a 5 mm Chemagnetics T3 probe. The Larmor frequency for ¹³C nuclei is 125.7 MHz. The ¹³C CPMAS (cross-polarization magic angle spinning) NMR spectra were recorded by using a contact time of 1 ms and at a spinning speed of 5 kHz. The ¹³C chemical shift was externally referenced to tetramethylsilane (TMS) at 0 ppm.

Thermogravimetric analysis (TGA) was conducted under nitrogen environment at a heating rate of 10 °C min⁻¹ from room temperature to 700 °C on a TA instrument Q50 thermogravimetric analyzer.

The hybrid polymer membrane was dipped in different electrolyte solvents for measurements of the extent of swelling. The swelling ratio was determined by $(W - W_0)/W_0 \times 100\%$, where W and W_0 are the weights of the wet and dry hybrid polymer membrane, respectively.

AC impedance spectroscopic measurements of the plasticized organic–inorganic hybrid electrolytes were performed using AUTOLAB/PGSTAT 302 frequency response analyzer over a frequency range of 100 kHz–1 Hz with an amplitude of 10 mV. All the specimens were sandwiched by two polished stainless steel blocking electrodes in argon atmosphere inside a glove box (Innovative technology, PL-HE-2GB with PL-HE-GP1 inert gas purifier) for conductivity tests. The measurements were performed in the temperature range of 10–80 °C, and the system was thermally equilibrated at each selected temperature for at least 1 h. Complex impedance plots (semi-circles) were computed from the raw experimental data. The ionic conductivity values (σ) have been obtained from the equation $\sigma = (1/R_b)(t/A)$, where R_b is the bulk resistance, t is the thickness of the electrolyte and A is the area of the electrode.

Linear sweep voltammetry (LSV) measurement was carried out in plasticized hybrid electrolyte membranes with different electrolyte solvents. A standard 2032 coin-cell hardware was used for

cell fabrication. Hybrid membranes were dried overnight at 70 °C in an oven and placed into an argon-filled glove box (Innovative technology, PL-HE-2GB) that contained <1 ppm oxygen and moisture. The PCEG-Y membrane was soaked in the electrolyte solutions for 10 min. The electrochemical stability of the plasticized hybrid polymer electrolytes was determined by LSV using stainless steel (SS) as a working electrode and lithium as counter and reference electrodes for a Li/plasticized hybrid polymer electrolyte/SS cell at a scan rate of 1 mV s⁻¹ from an open circuit potential to 7 V vs. Li/Li⁺.

Charge–discharge studies were carried out with WonATech WBCS3000 automatic battery cycler. Lithium metal (Alfa Products) was used as the anode. For the cathode preparation, initially NMC442 and LMO were mixed in the weight ratio of 7:3. Then the cathode was prepared by blade-coating a slurry of 88 wt.% NMC442/LMO mixture with 12 wt.% poly(vinylidene fluoride) (PVdF) binder in *N*-methyl-2-pyrrolidone (NMP) on aluminum foil, drying overnight at 120 °C in an oven, roller-pressing the dried coated foil, and punching out circular discs. The cycle tests of normal charge were carried out at a 0.2 C-rate between 2.8 and 4.2 V.

3. Results and discussion

3.1. Chemical and physical properties

Infrared spectroscopy was used to characterize the chain structure of the organic–inorganic hybrid membrane. Fig. 1 shows the FTIR spectra of pure ED2003, pure PEGDGE, pure PVdF–HFP, and the PCEG-5 and PCEG-10 hybrid membranes. The band observed at 3440 cm⁻¹ in PCEG-5 and PCEG-10 hybrid membranes was assigned to the hydrogen-bonded N–H stretching mode [38]. In pure PEGDGE, the band observed at 3540 cm⁻¹ was due to the O–H vibration, related to the water which was entrapped from the air by the sample. In pure ED2003, however, overlapping of O–H and N–H vibration gave rise to a broad band around that region. The peak at 2875 or 2876 cm⁻¹ which was due to the CH₂ stretching

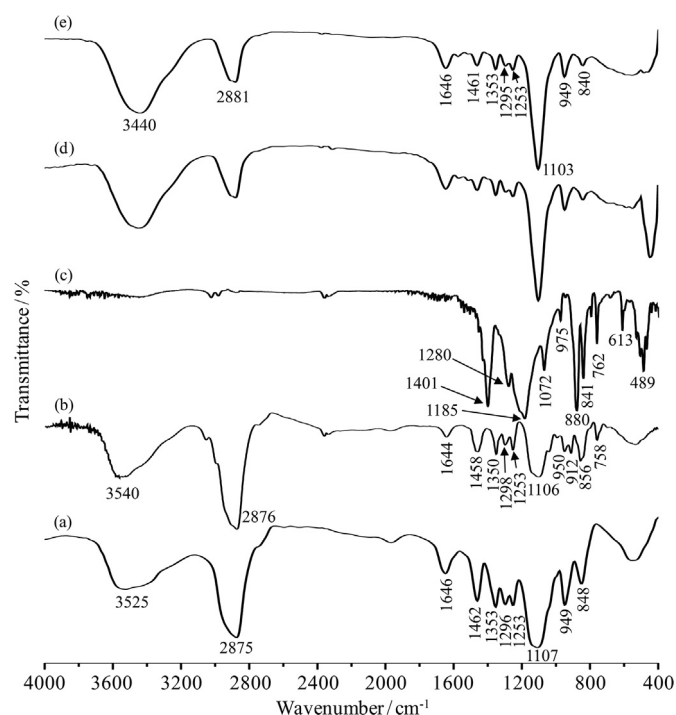


Fig. 1. FTIR spectra of (a) pure ED2003, (b) pure PEGDGE, (c) pure PVdF–HFP, and (d) PCEG-5 and (e) PCEG-10 hybrid membranes.

vibration of EO chain of ED2003 or PEGDGE, shifted to 2881 cm^{-1} in the hybrid membranes [39]. The band around 1646 or 1644 cm^{-1} was associated with the hydrogen bonded carbonyls. The bands around 1461 , 1353 , 1298 – 1295 and 1253 cm^{-1} were due to CH_2 scissoring, wagging and twisting vibrations of the polymers ED2003 and PEGDGE [40,41]. A major band associated with C–O–C stretching vibrations was observed around 1103 – 1107 cm^{-1} for the parent ED2003, PEGDGE and the hybrid polymer membrane [42]. The specific interaction between the fluorine in PVdF–HFP and the carbon connected to oxygen of ED2003 or PEGDGE, which can act as a Lewis base and a Lewis acid, respectively, shifted the band slightly toward lower frequency for the hybrid polymer membrane [43,44]. A band at 949 cm^{-1} with a medium intensity was assigned to the coupled vibration of C–C stretching and CH_2 rocking modes [45]. There is a strong possibility of Si–OH present in the hybrid membrane due to GLYMO which overlaps with the band frequency at 949 cm^{-1} . The bands due to the CH_2 rocking vibration of both PVdF–HFP and EO chain were observed at 840 cm^{-1} in the hybrid membrane. As seen in Fig. 1c, both α and β phase of the PVdF–HFP are present in the pure sample. The bands at 489 , 613 , 762 , 975 and 1401 cm^{-1} corresponding to the α phase of PVdF are absent in the hybrid organic–inorganic membrane. Instead, we observed the bands at 840 cm^{-1} and 1280 cm^{-1} (maybe overlap with the 1295 cm^{-1} band) belonging to the β phase of PVdF [46] in the hybrid membrane. This suggests that the highly ordered spherulitic structure of α phase is diminished or converted to fibrous β phase in the hybrid membrane. The appearance of only fibrous β phase of PVdF–HFP in the hybrid membrane paved the way for higher conductivity due to its lower crystallinity. In comparison to the pure components, the significant changes in the band positions and/or in the band magnitude of the hybrid indicate that there are some interactions among ED2003, PEGDGE, PVdF–HFP and GLYMO.

Solid-state ^{13}C CPMAS NMR experiments were performed to gain the information about the backbone structure of the hybrid membrane. Fig. 2 shows the ^{13}C CPMAS NMR spectra of the organic–inorganic hybrid membranes acquired at a short contact time of 1.0 ms. The most predominant peak at 70.5 ppm is assigned to the methylene carbons adjacent to the ether oxygens of the polymer chains of ED2003 and PEGDGE [42]. Because of the high concentrations of these moieties in ED2003 and PEGDGE, the signals associated with the carbon atoms of all the other functional

groups present in this matrix are relatively weak. The methyl carbon from the propylene oxide units appears at 17 ppm , while the peak at 43 ppm can be assigned to the methylene carbons in PVdF–HFP. The small peak around 120 ppm is assigned to the carbon atom of CF_2 . A very small ^{13}C signal at 150 ppm due to the central core CC is observed for the PCEG-5 sample, which disappeared while increasing the amount of PVdF–HFP in PCEG-10 as the CC concentration is relatively small in comparison to the amount of other constituents of the membrane. Two small peaks at 23 and 9 ppm are assigned to the methylene carbons in the α and β positions to the silicon atom of GLYMO, respectively. There is a smaller peak at 75 ppm due to the ether carbons in the PPG segments of ED2003. In addition, the peak at 72.8 ppm can be assigned to the carbons attached to ether oxygen atoms of GLYMO. The ^{13}C CPMAS NMR observations are consistent with the hybrid structure as illustrated in Scheme 1.

3.2. Thermal properties

TGA experiments were carried out to determine the thermal stability of the organic–inorganic hybrid electrolyte membranes. The TGA curves of the dry and plasticized electrolyte membranes of PCEG-5 and PCEG-10 are shown in Fig. 3. As shown in Fig. 3, there is almost no weight loss up to $220\text{ }^\circ\text{C}$ in the dry hybrid membranes, indicative of high thermal stability of the materials. After plasticization with 1 M LiPF_6 in EC/DEC, the hybrid electrolyte membranes show a steady behavior up to $100\text{ }^\circ\text{C}$ with no obvious weight loss. After $100\text{ }^\circ\text{C}$, the weight loss has slowly started and around 50% weight loss occurred between 100 and $400\text{ }^\circ\text{C}$, which may be due to the evaporation of electrolyte solvents EC (b.p. $260\text{ }^\circ\text{C}$) and DEC (b.p. $126\text{ }^\circ\text{C}$). Therefore, the plasticized hybrid electrolyte membrane is thermally stable at least up to $100\text{ }^\circ\text{C}$ and suitable as a separator for Li-ion polymer batteries within this temperature limit. It is noted that the weight loss is almost 100% (i.e., 0% retention) at $700\text{ }^\circ\text{C}$ for both of the dry PCEG-5 and PCEG-10 hybrid membranes, while the plasticized electrolyte membranes can retain around 40% weight at that temperature. At higher temperatures, the LiPF_6 salt decomposes to LiF and PF_5 , and the latter readily hydrolyzes to form HF and PF_3O [47]. It is possible that the decomposed products somehow restrict the weakening of C–O bonds, which resist the thermal degradation of the plasticized hybrid electrolyte membranes. A further study is needed to confirm this assumption.

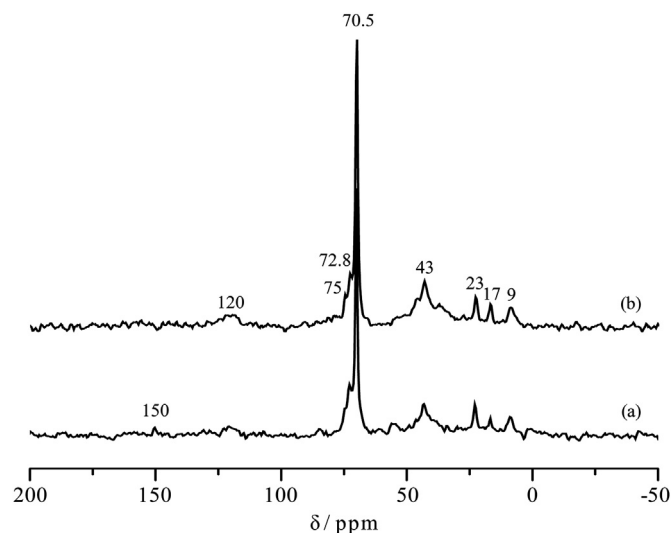


Fig. 2. ^{13}C CPMAS NMR spectra of (a) PCEG-5 and (b) PCEG-10 organic–inorganic hybrid membranes acquired at a contact time of 1.0 ms.

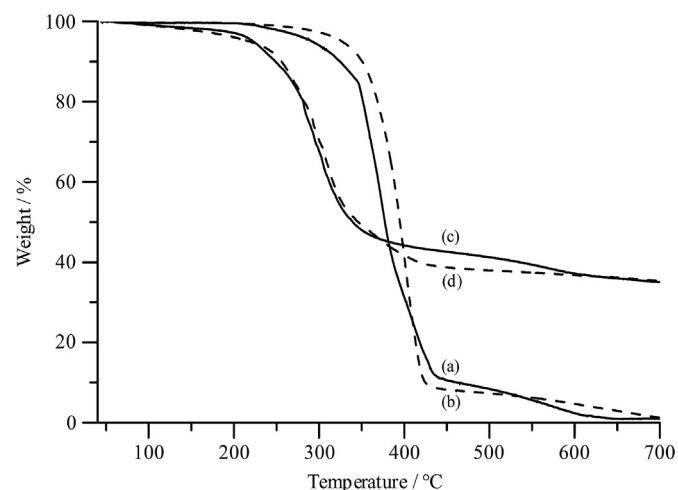


Fig. 3. TGA curves of dried (a) PCEG-5 and (b) PCEG-10 membranes and plasticized (c) PCEG-5 and (d) PCEG-10 electrolyte membranes in 1 M LiPF_6 in EC/DEC.

3.3. Swelling properties

In order to enhance the ionic conductivity, a faster and efficient uptake of liquid electrolyte by the hybrid membrane is required and the membrane should be mechanically and chemically stable. The swelling behavior as a function of soaking time is shown in Fig. 4 for the PCEG-5 sample in different electrolyte solvents. As seen in Fig. 4, the swelling ratio increases with the increase in soaking time and the swollen membranes are mechanically stable within the measured soaking time. All the hybrid membranes with different electrolyte solvents exhibit a maximum swelling ratio about 10–15 min of soaking time. Table 1 lists the percentages of swelling of the PCEG-5 and PCEG-10 samples in different electrolyte solvents. A maximum swelling percentage of 794% was achieved with 1 M LiClO₄ in EC/PC for the PCEG-5 sample, which is relatively higher than other reported gel polymer electrolytes [25,26,36,48–50]. The swelling ratio decreases for the PCEG-10 sample with increasing the amount of PVdF–HFP, due to its hardness in comparison to ED2003. Such a high value of swelling ratio is attributed to the typical branched structure of the hybrid membrane, which helps to absorb more electrolyte solvents. It was found that the swelling ratios followed the order: 1 M LiClO₄ in EC/PC (1:1, v/v) > 1 M LiOTf in EC/PC (1:1, v/v) > 1 M LiTFSI in EC/PC (1:1, v/v) > 1 M LiPF₆ in EC/DEC (1:1, v/v).

The electrolyte uptake of the membrane depends on the viscosity of the solvents as well as the compatibility of the solvents with the polymer. Estimation of viscosities of the solvent mixture in 1 M solution of salts is carried out to get a rough idea on the variation of swelling percentages in this hybrid membrane with different electrolyte solvents. Although the EC/DEC mixture has low viscosity ($\eta(\text{EC}) = 1.9$ cP and $\eta(\text{DEC}) = 0.75$ cP, η of the mixture = 1.325 cP) in comparison to EC/PC ($\eta(\text{EC}) = 1.9$ cP and $\eta(\text{PC}) = 2.53$ cP, η of the mixture = 2.215 cP) [8], DEC may not be totally compatible with the hybrid polymer structure. Further, the molecular structure of DEC is bigger than EC and PC, which may influence the absorption. Hence, a lower electrolyte uptake is obtained with EC/DEC than with EC/PC. Moreover, the dissociation constant of salts plays a role in the swelling behavior. As the dissociation constants follows the order LiTFSI > LiClO₄ > LiOTf, the LiTFSI salt dissociates more easily than LiClO₄, resulting in enhancement of the viscosity of the 1 M LiTFSI in EC/PC in comparison to 1 M LiClO₄ in EC/PC [51,52]. Therefore, the swelling ratio of the hybrid membrane in 1 M LiTFSI in EC/PC is lower than 1 M

Table 1

Swelling ratios (SR), ionic conductivities (σ , at 30 °C) and activation energies (E_a) of plasticized hybrid electrolytes in different electrolyte solvents.

Electrolyte solvents	PCEG-5			PCEG-10		
	SR, %	σ , mS cm ⁻¹	E_a , eV	SR, %	σ , mS cm ⁻¹	E_a , eV
1 M LiClO ₄ in EC/PC (1:1, v/v)	794	6.9	0.07	626	5.9	0.06
1 M LiOTf in EC/PC (1:1, v/v)	789	4.5	0.07	621	3.1	0.08
1 M LiTFSI in EC/PC (1:1, v/v)	744	3.1	0.08	580	2.3	0.09
1 M LiPF ₆ in EC/DEC (1:1, v/v)	670	2.3	0.09	571	2.1	0.09

LiClO₄ in EC/PC. Although the dissociation constant of LiClO₄ is slightly higher than LiOTf, the swelling ratios of the membranes with these electrolytes are almost the same at a longer soaking time.

The higher value of the electrolyte uptake is also due to the porous structure of the membrane as shown in the inset SEM image in Fig. 4. This porous structure efficiently retains the electrolyte solvent in these pores resulting in a higher swelling ratio.

3.4. Ionic conductivity measurements

To analyze the transport behavior in different electrolytes, the ionic conductivities of PCEG-5 and PCEG-10 hybrid membranes were measured after swelled in different electrolytes. Fig. 5 shows the temperature dependence of ionic conductivity of the PCEG-5 plasticized hybrid electrolytes swelled in different electrolyte solvents. The plot shows almost linear enhancement of conductivity with slight non-linear variation at high temperatures suggesting that conductivity behavior is predominantly Arrhenius in nature. The Arrhenius equation can be described as,

$$\sigma = \sigma_0 \exp(-E_a/kT) \quad (1)$$

where σ is the ionic conductivity, σ_0 is the pre-exponential factor, E_a is the activation energy and k is the Boltzmann's constant. The ionic conductivities at 30 °C and activation energies (E_a) of the PCEG-5 and PCEG-10 samples in different electrolyte solvents are listed in Table 1. As seen in Table 1, the maximum ionic conductivity value of 6.9×10^{-3} S cm⁻¹ has obtained at 30 °C from the PCEG-5 plasticized

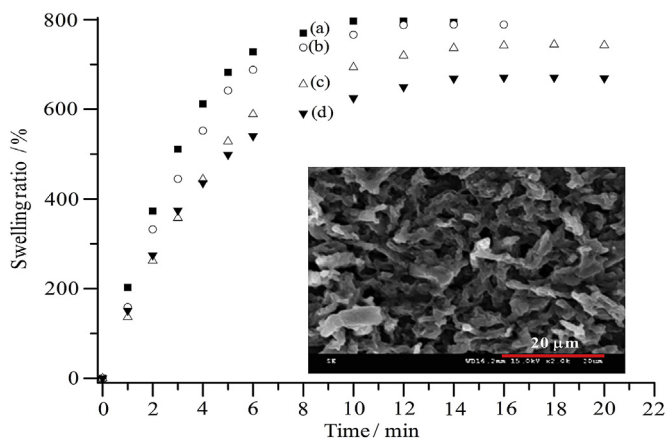


Fig. 4. Swelling behavior of PCEG-5 hybrid membrane with different electrolyte solvents, (a) 1 M LiClO₄ in EC/PC (1:1, v/v), (b) 1 M LiOTf in EC/PC (1:1, v/v), (c) 1 M LiTFSI in EC/PC (1:1, v/v) and (d) 1 M LiPF₆ in EC/DEC (1:1, v/v). The SEM image of the microporous structure of the membrane is shown as inset.

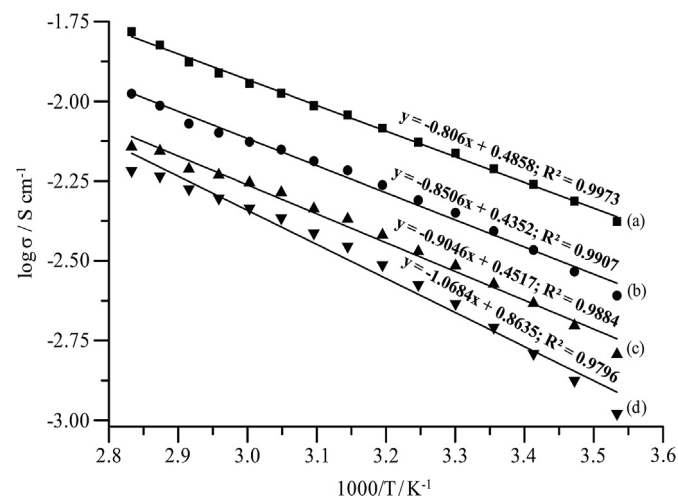


Fig. 5. Temperature dependence of ionic conductivity with Arrhenius fitting of plasticized PCEG-5 hybrid electrolyte membranes with different electrolyte solvents, (a) 1 M LiClO₄ in EC/PC (1:1, v/v), (b) 1 M LiOTf in EC/PC (1:1, v/v), (c) 1 M LiTFSI in EC/PC (1:1, v/v) and (d) 1 M LiPF₆ in EC/DEC (1:1, v/v).

hybrid electrolyte with 1 M LiClO₄ in EC/PC. Then, the conductivity decreases in the order of 1 M LiOTf in EC/PC > 1 M LiTFSI in EC/PC > 1 M LiPF₆ in EC/DEC. The same type of conductivity trend is observed with the PCEG-10 plasticized hybrid electrolytes. The ionic conductivity enhancement is directly related to the swelling ratio of the membrane in different electrolyte solvents. The most ion conductive PCEG-5 sample plasticized with 1 M LiClO₄ in EC/PC also exhibits the highest value of swelling ratio. It is found that the conductivity decreases with the decrease in the swelling ratio. This observation suggests that the liquid electrolytes are entrapped in the pores of the polymer matrix and then penetrated into the polymer chains for swelling the amorphous domains [53,54]. In this type of hybrid system, the lithium ions can move through the polymer electrolyte in three ways, namely through liquid electrolyte stored in the pores, amorphous domains swelled by liquid electrolyte, and along the polymer chains. The movement of the lithium ions along the polymer chains is much slower than the movement through the pores and amorphous domains. As there is plenty of the solvent retained in the hybrid electrolyte membrane for coordination to the Li⁺ cations and the carbonyl solvents are better for coordinating with the cations than with the ether oxygens, the pores filled with liquid electrolyte and swelled amorphous domains are the main transfer channels of the lithium ions, which are responsible for the reported ionic conductivity. Moreover, the interconnected pores formed between spherulites of PVdF–HFP, which act as channels for lithium ion movement, helps further enhancement in ionic conductivity. In the membranes with high electrolyte uptakes, these interconnected pore channels are filled with liquid electrolytes, and thus the Li⁺ ions can move faster through these channels to give higher ionic conductivity. The lower *E_a* value of 0.07–0.09 eV (Table 1) also suggests the high ionic conductivity of the plasticized hybrid electrolyte samples.

3.5. Linear sweep voltammetry

Electrochemical window is an important parameter to evaluate the stability of the polymer electrolyte. For lithium ion batteries, it is necessary for the hybrid electrolyte to have high electrochemical stability. The electrochemical stability of the PCEG-5 plasticized hybrid polymer electrolytes with different electrolyte solvents was investigated by linear sweep voltammetry (LSV) to endure the operating voltage of the battery system. Fig. 6 displays the linear sweep voltammograms of the PCEG-5 plasticized hybrid electrolytes in different electrolyte solvents. A very low background current was measured in the potential region between 0 and 4.3 V for the cell prepared with SS electrode. This small current might be attributed to the change of the stainless steel surface [55]. Upon reaching around 4.3 V, a considerable current began to flow, indicating the onset of the electrolyte decomposition process. Therefore, the onset decomposition voltage of the hybrid electrolyte is around 4.3 V vs. Li/Li⁺ with the SS electrode. The hybrid electrolyte membranes with all the tested electrolyte solvents show almost the same value of the electrochemical stability window. Therefore, this hybrid electrolyte can be used in the lithium ion polymer battery, where the cell voltage is around 4 V.

3.6. Charge–discharge behavior

Although the ionic conductivity of the hybrid electrolyte membranes with the LiClO₄, LiOTf and LiTFSI based salts were higher than the LiPF₆ based salt, for safety reason (e.g., explosion of cell due to strong oxidizing character of the salts) the standard procured electrolyte of 1 M LiPF₆ in EC/DEC was used for charge–discharge testing of the cell. To evaluate the electrochemical performance of the lithium ion polymer battery with the hybrid

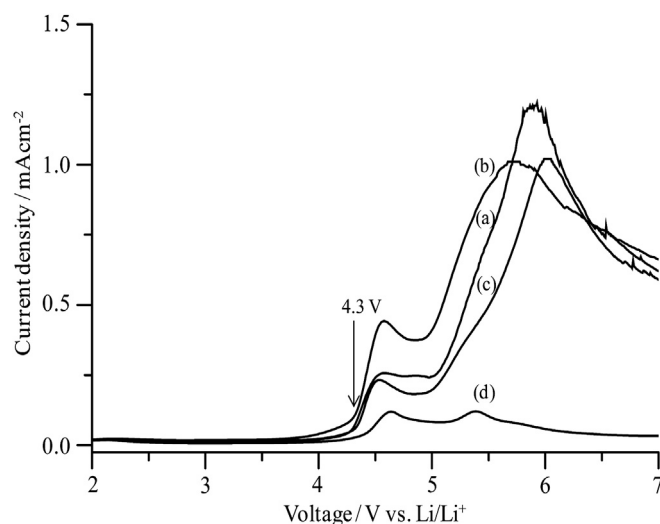


Fig. 6. Linear sweep voltammetry curves of the cell prepared with plasticized PCEG-5 hybrid electrolytes with different electrolyte solvents, (a) 1 M LiClO₄ in EC/PC (1:1, v/v), (b) 1 M LiOTf in EC/PC (1:1, v/v), (c) 1 M LiTFSI in EC/PC (1:1, v/v) and (d) 1 M LiPF₆ in EC/DEC (1:1, v/v).

electrolyte, Li/PCEG-5(1 M LiPF₆ in EC/DEC)/NMC442-LMO battery was assembled. The assembled battery was subjected to cycle tests with upper voltage limit of 4.2 V and lower voltage limit of 2.8 V at a current rate of 0.2 C. Fig. 7 shows the 1st, 50th and 100th cycles charge–discharge behavior of the lithium ion polymer battery. The coulombic efficiency of the first cycle was about 98.9%, which increased to 99.5% at the 50th cycle and then slightly decreased to 98% at the 100th cycle. The irreversible capacity loss observed in these cycles is caused by the formation of passivation film on the surface of the lithium electrode due to the decomposition of electrolyte. The formation of passivation layer consumes a part of the anode capacity corresponding to an irreversible capacity loss. The passive layer reduces the charge transfer in the lithium electrode and the diffusion rate of Li⁺ ion in the Li/hybrid electrolyte interface becomes very slow. This passivation film prevents the electrolyte from further reduction by the active lithium, and the coulombic efficiency is almost stable in between 98 and 99% with the entire cycle numbers.

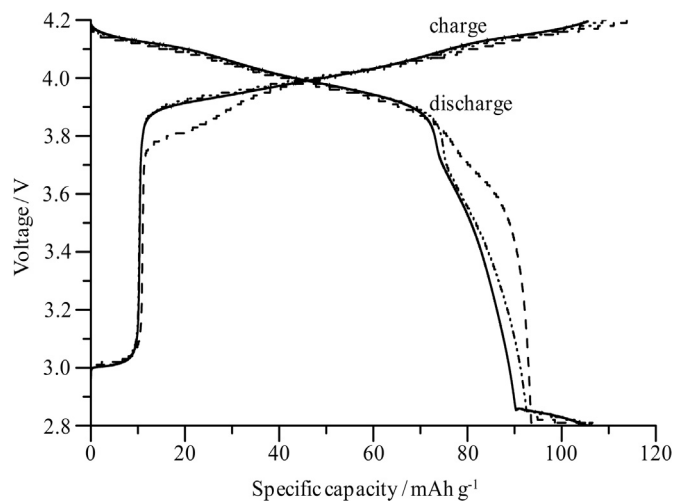


Fig. 7. Galvanostatic charge–discharge curves of 1st (solid line), 50th (dash) and 100th (dash double dot) cycles for the Li/PCEG-5(1 M LiPF₆ in EC/DEC)/NMC442-LMO cell.

The discharge capacity as a function of cycle number of the lithium ion polymer battery with the PCEG-5 (1 M LiPF₆ in EC/DEC) hybrid electrolyte is shown in Fig. 8. The initial discharge capacity of the cell is 115 mAh g⁻¹ which is increased in between to 119 mAh g⁻¹ and then slowly decreases to 106 mAh g⁻¹ at the 100th cycle due to the formation of Li/hybrid electrolyte interface layer [56]. At the 100th cycle, about 92% of the initial discharge capacity is retained without any sign of cell failure. It suggests that during the cycling, the physical changes in the active materials and the passivation film on the surface of the electrode gradually increase cell internal resistance and block the charge transfer reaction between the Li electrode and the hybrid electrolyte which results in the discharge capacity loss with cycling. The observed minor fluctuation in discharge capacity values with cycle numbers may be due to the unstable and non-uniform solid electrolyte interphase (SEI) layer. Temperature variation in our instrument's cell testing pods may also cause slight changes in the SEI layer, which is responsible for a minor fluctuation in discharge capacity values [57]. For comparison purpose, another cell was assembled with commercial polyethylene (PE) separator membrane with 40% porosity and 25 μm thickness. It is observed that discharge capacity of PE based cell decreases from 126 mAh g⁻¹ to 97 mAh g⁻¹ within 100 cycles. Therefore, only 77% of initial discharge capacity is retained after 100 cycles with the standard PE separator. As the capacity loss is only 8% up to 100th cycles for the PCEG-5 hybrid electrolyte based cell, it suggests a good compatibility of the hybrid polymer matrix with the liquid electrolyte to provide almost stable cycle life of the hybrid electrolyte based cell.

Although the use of LiClO₄ based electrolyte in cell may cause explosion, we have tested the cell with the PCEG-5 electrolyte membrane in 1 M LiClO₄ in EC/PC with extreme precaution as this membrane exhibits the highest ionic conductivity for this electrolyte system. Fig. 9 shows the discharge capacity as a function of cycle number for the cell with the above mentioned electrodes. Although the first cycle discharge capacity value of 122 mAh g⁻¹ is higher than the PCEG-5 electrolyte membrane with 1 M LiPF₆ in EC/DEC, the discharge capacity value decreases rapidly to 113 mAh g⁻¹ within three cycles and then gradually reduces to 41 mAh g⁻¹ at 10 cycles. This may be due to the high active surface originated from the dendritic morphology formed on the lithium anode after the first charge, which can promote a larger consumption of the lithium by the decomposition reactions of EC, PC and ClO₄⁻ during a

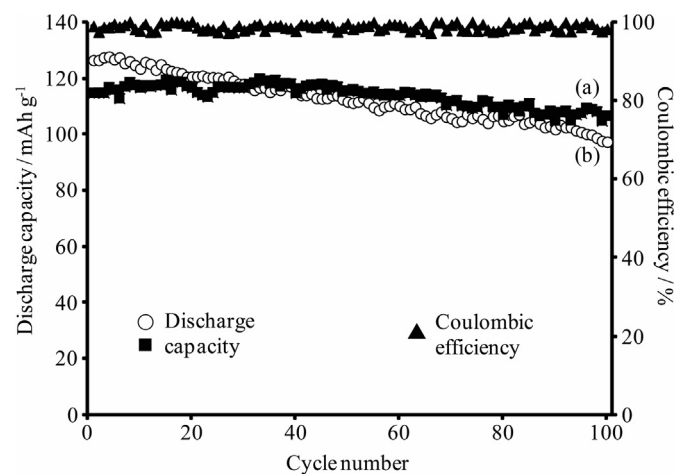


Fig. 8. Cycling behaviors of the cells fabricated with Li anode and NMC442/LMO cathode and with (a) PCEG-5 (1 M LiPF₆ in EC/DEC) electrolyte membrane and (b) standard PE separator membrane. Coulombic efficiency is measured for the PCEG-5 electrolyte membrane with 1 M LiPF₆ in EC/DEC.

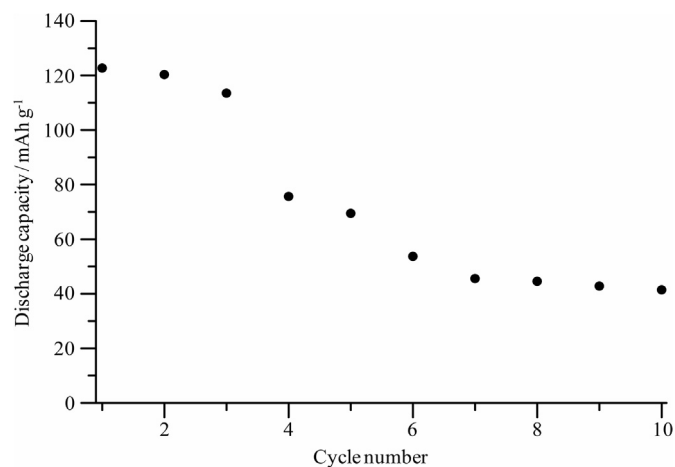


Fig. 9. Cycling behaviors of the cell fabricated with Li anode and NMC442/LMO cathode with PCEG-5 electrolyte membrane in 1 M LiClO₄ in EC/PC.

prolonged cycling and thereby produces a thicker SEI layer resulting in a longer diffusion path of the lithium ions. Besides, this dendritic lithium can perforate the polymer electrolyte, resulting in an internal short-circuit of the cell. Therefore, the PCEG-5 hybrid electrolyte membrane with 1 M LiPF₆ in EC/DEC is a better candidate in comparison to 1 M LiClO₄ in EC/PC for the use in lithium ion polymer batteries with good cycle life and discharge capacity.

4. Conclusions

A highly conductive plasticized organic–inorganic hybrid electrolyte membrane based on ED2003, PEGDGE, CC, PVdF–HFP and GLYMO has been synthesized. The TGA result confirms that the plasticized hybrid electrolyte membrane is thermally stable up to 100 °C with no obvious weight loss. The hybrid electrolyte membrane shows remarkable swelling ratios in the range of 670–800% in different electrolyte solvents within 10–15 min of soaking time. The plasticized hybrid electrolyte membrane exhibits a high ionic conductivity value of 6.9×10^{-3} S cm⁻¹. The test cell with NMC442/LMO cathode and lithium anode carries an initial discharge capacity value of 115 mAh g⁻¹ at 0.2 C. The characteristic electrochemical properties open new possibilities for such type of organic–inorganic hybrid electrolytes for applications in lithium polymer batteries.

Acknowledgment

The financial support of this work by the National Science Council of Taiwan is gratefully acknowledged.

References

- [1] J.M. Tarascon, M. Armand, *Nature* 414 (2001) 359–367.
- [2] B. Scrosati, J. Hassoun, Y.-K. Sun, *Energy Environ. Sci.* 4 (2011) 3287–3295.
- [3] M. Armand, J.M. Tarascon, *Nature* 451 (2008) 652–657.
- [4] V. Etacheri, R. Marom, R. Elazari, G. Salitra, D. Aurbach, *Energy Environ. Sci.* 4 (2011) 3243–3262.
- [5] E. Quartarone, P. Mustarelli, *Chem. Soc. Rev.* 40 (2011) 2525–2540.
- [6] V.D. Noto, S. Lavina, G.A. Giffin, E. Negro, B. Scrosati, *Electrochim. Acta* 57 (2011) 4–13.
- [7] R.C. Agrawal, G.P. Pandey, *J. Phys. D: Appl. Phys.* 41 (2008), 223001(1–18).
- [8] K. Xu, *Chem. Rev.* 104 (2004) 4303–4417.
- [9] F. Croce, M.L. Focarete, J. Hassoun, I. Meschini, B. Scrosati, *Energy Environ. Sci.* 4 (2011) 921–927.
- [10] S. Oh, D.W. Kim, C. Lee, M.-H. Lee, Y. Kang, *Electrochim. Acta* 57 (2011) 46–51.
- [11] M. Higa, K. Yaguchi, R. Kitani, *Electrochim. Acta* 55 (2010) 1380–1384.
- [12] R. Prasanth, V. Aravindan, M. Srinivasan, *J. Power Sources* 202 (2012) 299–307.

- [13] M. Kunze, Y. Karatas, H.-D. Wiemhöfer, H. Eckert, M. Schönhoff, *Phys. Chem. Chem. Phys.* 12 (2010) 6844–6851.
- [14] D. Saikia, Y.-H. Chen, Y.-C. Pan, J. Fang, L.-D. Tsai, G.T.K. Fey, H.-M. Kao, *J. Mater. Chem.* 21 (2011) 10542–10551.
- [15] A.M. Rocco, de A. Carias, R.P. Pereira, *Polymer* 51 (2010) 5151–5164.
- [16] İ.B. Pehlivan, P. Georén, R. Marsal, C.G. Granqvist, G.A. Niklasson, *Electrochim. Acta* 57 (2011) 201–206.
- [17] C.M. Costa, L.C. Rodrigues, V. Sencadas, M.M. Silva, S. Lancers-Méndez, *Solid State Ionics* 217 (2012) 19–26.
- [18] D. Zhang, H. Yan, H. Zhang, Z. Zhu, Qilu, *Solid State Ionics* 199–200 (2011) 32–36.
- [19] H.-J. Ha, Y.H. Kwon, J.Y. Kim, S.-Y. Lee, *Electrochim. Acta* 57 (2011) 40–45.
- [20] Y.T. Chen, Y.C. Chuang, J.H. Su, H.C. Yu, Y.W. Chen-Yang, *J. Power Sources* 196 (2011) 2802–2809.
- [21] J. Zhang, X. Huang, H. Wei, J. Fu, Y. Huang, X. Tang, *J. Appl. Electrochem.* 40 (2010) 1475–1481.
- [22] M. Patel, M.U.M. Patel, A.J. Bhattacharyya, *ChemSusChem* 3 (2010) 1371–1374.
- [23] A. Sarnowska, I. Polska, L. Niedzicki, M. Marcinek, A. Zalewska, *Electrochim. Acta* 57 (2011) 180–186.
- [24] S. Rajendran, M.R. Prabhu, M. Usha Rani, *J. Power Sources* 180 (2008) 880–883.
- [25] D. Saikia, H.-Y. Wu, Y.-C. Pan, C.-P. Lin, K.-P. Huang, K.-N. Chen, G.T.K. Fey, H.-M. Kao, *J. Power Sources* 196 (2011) 2826–2834.
- [26] A. Subramania, N.T. Kalyana Sundaram, A.R. Sathiy Priya, G.V. Kumar, *J. Membr. Sci.* 294 (2007) 8–15.
- [27] C.-C. Liao, H.-Y. Wu, D. Saikia, Y.-C. Pan, Y.-K. Chen, G.T.K. Fey, H.-M. Kao, *Macromolecules* 41 (2008) 8956–8959.
- [28] Y.-H. Liang, C.-Y. Hung, C.-C. Wang, C.-Y. Chen, *J. Power Sources* 188 (2009) 261–267.
- [29] P. Barbosa, L. Rodrigues, M. Silva, M. Smith, A. Gonçalves, E. Fortunato, *J. Mater. Chem.* 20 (2010) 723–730.
- [30] Y.-C. Pan, D. Saikia, J. Fang, L.-D. Tsai, G.T.K. Fey, H.-M. Kao, *Electrochim. Acta* 56 (2011) 8519–8529.
- [31] D.M. Tigelaar, M.A.B. Meador, J.D. Kinder, W.R. Bennett, *Macromolecules* 39 (2006) 120–127.
- [32] L.M. Bronstein, R.L. Karlinsey, K. Ritter, C.G. Joo, B. Stein, J.W. Zwanziger, *J. Mater. Chem.* 14 (2004) 1812–1820.
- [33] M. Marczewski, M. Piszcz, A. Plewa-Marczewska, G.Z. Żukowska, A. Pietrzykowski, M. Siekierski, *Electrochim. Acta* 55 (2010) 1338–1346.
- [34] W.-J. Liang, Y.-P. Chen, C.-P. Wu, P.-L. Kuo, *J. Appl. Polym. Sci.* 100 (2006) 1000–1007.
- [35] Y. Ding, P. Zhang, Z. Long, Y. Jiang, F. Xu, W. Di, *J. Membr. Sci.* 329 (2009) 56–59.
- [36] Z. Ren, Y. Liu, K. Sun, X. Zhou, N. Zhang, *Electrochim. Acta* 54 (2009) 1888–1892.
- [37] A.M. Stephan, K.S. Nahm, T.P. Kumar, M.A. Kulandainathan, G. Ravi, J. Wilson, *J. Power Sources* 159 (2006) 1316–1321.
- [38] D. Saikia, H.-Y. Wu, Y.-C. Pan, C.-C. Liao, C.-F. Chen, G.T.K. Fey, H.-M. Kao, *Electrochim. Acta* 54 (2009) 7156–7166.
- [39] L.S. Teo, C.Y. Chen, J.F. Kuo, *Macromolecules* 30 (1997) 1793–1799.
- [40] P. Patnaik, *Dean's Analytical Chemistry Handbook*, second ed., McGraw-Hill, New York, 2004.
- [41] D.L. Pavia, G.M. Lampman, G.S. Kriz, *Introduction to Spectroscopy*, Harcourt College Publication, USA, 2001.
- [42] H.M. Kao, T.T. Hung, G.T.K. Fey, *Macromolecules* 40 (2007) 8673–8683.
- [43] C.G. Wu, M.I. Lu, H.J. Chuang, *Polymer* 46 (2005) 5929–5938.
- [44] Y.J. Wang, D. Kim, *J. Power Sources* 166 (2007) 202–210.
- [45] M.M. Silva, V. de Zea Bermudez, L.D. Carlos, A.P.P. de Almeida, M.J. Smith, *J. Mater. Chem.* 9 (1999) 1735–1740.
- [46] C.-H. Du, B.-K. Zhu, Y.-Y. Xu, *J. Mater. Sci.* 41 (2006) 417–421.
- [47] E. Sloop, J.K. Pugh, S. Wang, J.B. Kerr, K. Kinoshita, *Electrochem. Solid State Lett.* 4 (2001) A42–A44.
- [48] M.M. Rao, J.S. Liu, W.S. Li, Y. Liang, D.Y. Zhou, *J. Membr. Sci.* 322 (2008) 314–319.
- [49] N.T. Kalyana Sundaram, A. Subramania, *Electrochim. Acta* 52 (2007) 4987–4993.
- [50] Q. Xiao, X. Wang, W. Li, Z. Li, T. Zhang, H. Zhang, *J. Membr. Sci.* 334 (2009) 117–122.
- [51] M. Ue, *J. Electrochem. Soc.* 141 (1994) 3336–3342.
- [52] W.A. Henderson, *Macromolecules* 40 (2007) 4963–4971.
- [53] Y. Saito, H. Kataoka, E. Quartarone, P. Mustarelli, *J. Phys. Chem. B* 106 (2002) 7200–7204.
- [54] Z. Li, G. Su, X. Wang, D. Gao, *Solid State Ionics* 176 (2005) 1903–1908.
- [55] D.Y. Zhou, G.Z. Wang, W.S. Li, G.L. Li, C.L. Tan, M.M. Rao, Y.H. Liao, *J. Power Sources* 184 (2008) 477–480.
- [56] H.-H. Kuo, W.-C. Chen, T.-C. Wen, A. Gopalan, *J. Power Sources* 110 (2002) 27–33.
- [57] P. Verma, P. Maire, P. Novák, *Electrochim. Acta* 55 (2010) 6332–6341.